THE JOURNAL OF PHYSICAL CHEMISTRY C

ARTICLE

pubs.acs.org/JPCC

$NiCo_2$ Alloys: Controllable Synthesis, Magnetic Properties, and Catalytic Applications in Reduction of 4-Nitrophenol

Kong-Lin Wu, Xian-Wen Wei,* Xian-Min Zhou, De-Hong Wu, Xiao-Wang Liu, Yin Ye, and Qi Wang

College of Chemistry and Materials Science, Key Laboratory of Functional Molecular Solids, the Ministry of Education, Anhui Laboratory of Molecule-Based Materials, Anhui Normal University, Wuhu 241000, People's Republic of China

Supporting Information

ABSTRACT: Dendritic $Ni_{33.8}Co_{66.2}$ alloy microstructures with hexagonal closed-packed phase have been prepared in large-scale by a simple and facile solution phase chemical route, while flowerlike $Ni_{33.4}Co_{66.6}$ in size of 2.5−5.5 μm was synthesized by solvothermal routes. Experimental results show that the reaction temperature, total concentration of $[Ni^{2+}]$ + $[Co^{2+}]$, and kinds of solvent and surfactants are key factors for controlling the morphology and crystal phase of the NiCo alloy. The possible formation mechanism for the $Ni_{33.8}Co_{66.2}$ dendrites has been discussed. Magnetic measurements revealed that both of the $NiCo_2$ alloys obtained are ferromagnetic at room temperature. The saturation magnetization value of the $Ni_{33.8}Co_{66.2}$ dendrites (163.55 emu/g) is lower than that of the flowerlike $Ni_{33.4}Co_{66.6}$ (195.79 emu/g), but the $Ni_{33.8}Co_{66.2}$ dendritic structures exhibit an enhanced coercivity value. $NiCo_2$ alloys with different shapes ($Ni_{33.8}Co_{66.2}$ dendrites and flowerlike $Ni_{33.4}Co_{66.6}$) have been used as reusable heterogeneous catalysts to reduce 4-nitrophenol (4-NP) into 4-aminophenol (4-AP) by $NaBH_4$. The kinetic data indicate that $Ni_{33.8}Co_{66.2}$ dendrites are catalytically more active than the flowerlike $Ni_{33.4}Co_{66.6}$ probably due to its larger surface-to-volume ratio and surface areas, since their Brunauer−Emmett−Teller surface areas are 32.68 and 20.66 m^2/g, respectively.

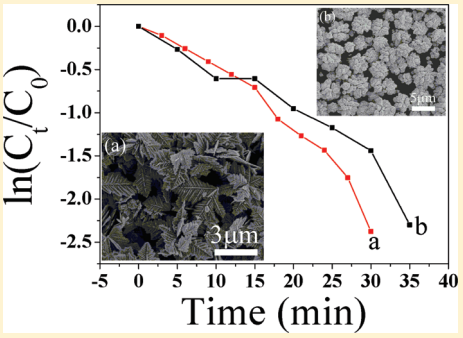

INTRODUCTION

Magnetic micro/nanostructures have attracted intensive interests because of their excellent physical, catalytic, and magnetic properties and their crucial applications in diverse fields, including high-density magnetic storage devices, magnetic resonance imaging, magnetic fluids, magnetic sensors, catalytic, environmental remediation, and biological applications. As one of important magnetic metal alloys, NiCo alloys have many superior properties,[1−7] which have been used for some high-temperature electrochemical devices, such as solid oxide fuel cells,[8] and some electromagnetic devices, such as magnetic recording devices, magcards, and ferrofluid dynamotors.[9] In recent years, various methods had been developed to prepare NiCo alloys with different morphologies, for example, $Ni_{70}Co_{30}$ nanorings,[10] NiCo nanochains,[11] $Ni_{20}Co_{80}$ and NiCo nanowires,[12−16] NiCo nanodumbbells,[12] $Ni_{19}Co_{81}$ nanotubes array,[17] nanoneedle-like NiCo,[18] handkerchief-like $Ni_{82}Co_{18}$,[19] $Ni_{49}Co_{51}$ spheres,[20] $Ni_{10}Co_{90}$ and NiCo nanoparticles,[4,21−23] and NiCo films[2,5,24−26] have been successfully synthesized by hydro/solvothermal method,[10,11,21] polyol process,[2,4,12,13,15] electrodeposition and template-approach,[5,7,14,16,17,25] mechanical alloying,[6] microemulsion system,[18,19] spray pyrolysis,[20] sol−gel technique,[22] chemical vapor deposition,[24] and so forth. Normally, chemical synthesis technique could overcome the drawbacks of high energy or costly reagents and had formed a basis for the synthesis of various alloy nanoparticles.[27] It is still a challenge to fully control the morphology of Ni−Co alloys with dendritic fractals, since dendritic fractals structures cannot only provide a framework for the study of disordered systems but also can be used as catalysts whose activity and selectivity are strongly dependent on the morphology of the structures.[28−31] Up to now, various dendritic metal and alloys nano/microstructures have been reported, including Pd,[31,32] Ag,[33] Au,[34,35] Ni,[36,37] Co,[38,39] Cu,[40,41] Pb−Te,[42] Ag−Pd,[43] Pt−Pb,[28] CuNi,[29] Pd−Cd,[30] and $FeNi_3$.[44] But, there is no report on NiCo alloy dendrites.

4-Aminophenol (4-AP) is an important intermediate in the preparation of several analgesic and antipyretic drugs such as paracetamol, acetanilide, phenacetin, and so forth, and it is used as a dyeing agent, a photographic developer, a corrosion inhibitor in paints, and an anticorrosion-lubricating agent in fuels for two-cycle engines. Recently, several heterogeneous catalysts containing noble metal such as Au,[45−48] Ag,[48−50] Pd,[51] Pt/C,[52] Au−SiO_2,[53] Ag−TiO_2,[54] and Pt−Ni[55] have been used for the reduction of 4-nitrophenol (4-NP) to 4-aminophenol in the presence of $NaBH_4$. However, the problems are that there is a high cost due to the usage of noble metal and usually carries are needed to avoid the nanoparticles aggregation during the reduction. Therefore, the direct catalytic reduction of 4-NP to 4-AP by $NaBH_4$ and cheap Ni-based transition metal catalysts could be an attractive and effective route, although hydrogenation of 4-NP in

Received: February 19, 2011
Revised: July 13, 2011
Published: July 15, 2011

the presence of various heterogeneous metal catalysts such as Raney Ni,[56] Ni,[57] Ni/Al_2O_3,[58] and Ni/TiO_2[59] under high pressure of H_2 and reduction of 4-NP by hydrazine in ethanol−water in the presence of Raney nickel[60] have been studied. It is still a challenge to use NiCo alloy as a highly efficient and reusable heterogeneous catalyst in this reaction.

Herein, we report a facile solution phase reduction route to Ni−Co alloys with dendritic structures in large scale by reduction of nickel chloride and cobalt chloride with hydrazine at 55 °C for 30 min using ethanol as solvent in the presence of cetyltrimethyl ammonium bromide (CTAB). The dendritic $Ni_{33.8}Co_{66.2}$ alloys were first used as recyclable, low cost, and environmentally benign catalyst in the reduction of 4-NP to 4-AP by $NaBH_4$, which were compared with flowerlike $Ni_{33.4}Co_{66.6}$, and both showed good catalytic properties and can be easy separated by a magnet from the solution for recycling. The kinetic data indicate that $Ni_{33.8}Co_{66.2}$ dendrites are catalytically more active than flowerlike $Ni_{33.4}Co_{66.6}$.

EXPERIMENTAL SECTION

Synthesis of Dendritic $Ni_{33.8}Co_{66.2}$ Alloys. In a typical procedure, $NiCl_2·6H_2O$ (2 mmol), $CoCl_2·6H_2O$ (4 mmol), and cetyltrimethyl ammonium bromide (CTAB, 1 mmol) were in order dissolved in 50 mL of absolute ethanol solution. After being under magnetic stirring for 30 min at room temperature, the above mixture was heated to 55 °C, and a solution composed of 15 mL of hydrazine hydrate ($N_2H_4·H_2O$, 80 wt %) and 0.03 mol of sodium hydroxide (NaOH) was added. The mixture color changed from dark blue to pink, then to milk white. After reaction for 30 min, the black fluffy solid products were collected by an external magnet, washed with distilled water and ethanol several times under ultrasonic, and then dried in a vacuum oven at 60 °C for 4 h. By using the same procedures, the concentrations of total metal ion and CTAB, reaction temperature, different surfactants and solvents, and time scale were varied to obtain particles with a desired morphology, size, phase, and compositions.

Synthesis of Flowerlike $Ni_{33.4}Co_{66.6}$ Alloy. In a typical procedure, $NiCl_2·6H_2O$ (1 mmol), $CoCl_2·6H_2O$ (2 mmol), and sodium dodecyl benzenesulfonate (SDBS, 0.5 mmol) were added to 40 mL of absolute ethanol at room temperature, and then, 0.015 mol of NaOH and 5 mL of hydrazine hydrate ($N_2H_4·H_2O$, 80 wt %) were orderly added under magnetic stirring. At last, the above solution was transferred to a 60 mL Teflon-lined stainless steel autoclave. The autoclave was sealed and maintained at 120 °C for 10 h. After the solution was cooled to room temperature, the black fluffy solid products were collected, washed with distilled water and ethanol several times under ultrasonic, and then dried in a vacuum oven at 60 °C for 4 h.

All the reagents used were analytical grade and used without further purification.

Material Characterization. The structural information on the samples was collected by X-ray powder diffraction (XRD) measurements that were carried out on a Shimadzu XRD-6000 X-ray diffractometer (Cu Kα radiation, λ = 1.5406 Å) with 2θ value from 30° to 80° at a scanning rate of 0.02°/s. The operation voltage and current were kept at 40 kV and 30 mA, respectively. The chemical composition (atomic percent) of the samples was determined by energy-dispersive X-ray (EDX) spectrometry (Hitachi S-4800 Japan). Morphologies of the samples were studied by scanning electron microscopy (SEM) (Hitachi S-4800 Japan). Transmission electron microscopy (TEM) and high-resolution transmission electron microscopy (HRTEM) were performed using a JEM-2010 microscope operated at 200 kV. Magnetic measurements were carried out at room temperature using a vibrating sample magnetometer (VSM, BHV-55) with a maximum magnetic field of 5 kOe. The UV−vis measurements were performed on a U4100 (Hitachi, Japan) spectrophotometer. Nitrogen adsorption experiments of as-synthesized samples were measured at 77 K on a Micromeritics ASAP 2020 system.

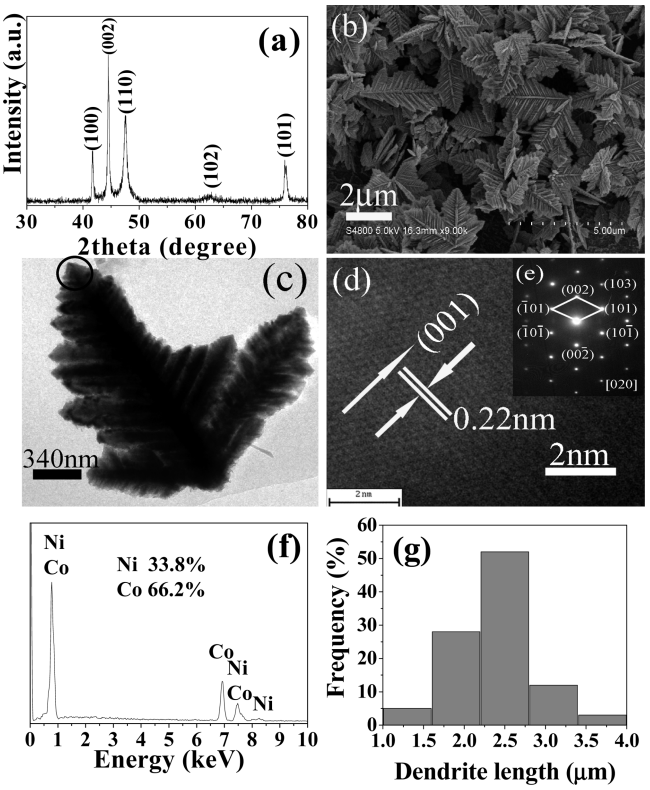

Figure 1. Integrated characterization of $Ni_{33.8}Co_{66.2}$ dendrites obtained by reduction of 0.04 M Ni^{2+} and 0.08 M Co^{2+} with hydrazine at 55 °C for 30 min in the presence of 0.01 M CTAB: (a) XRD pattern; (b) SEM image; (c) TEM image; (d) HRTEM image; (e) the corresponding SAED pattern taken from the tip of the trunk or branch in panel c; (f) EDX spectrum; (g) size distribution taken from the corresponding SEM image shown in panel b.

Catalytic Reaction. In a typical catalytic reaction, 10 mL (1.0×10^{-4} M) of aqueous solution of 4-NP and 10 mL (100 mg/L) of aqueous Ni−Co alloy colloidal suspensions were mixed together and then purged with argon for 10 min to remove the dissolved oxygen. Next, 10 mL (6×10^{-2} M) of aqueous $NaBH_4$ solution purged with argon was added to the reaction mixture, and time-dependent absorption spectra were recorded in the UV−vis spectrophotometer at 20 °C.

RESULTS AND DISCUSSION

Dendritic Ni−Co Alloy. The phase structure and purity of the as-synthesized samples were examined by X-ray powder diffraction (XRD). Figure 1a shows the XRD pattern of the typical Ni−Co alloy structures obtained by reaction of 0.04 M Ni^{2+} and 0.08 M Co^{2+} in absolute ethanol with hydrazine at 55 °C for

30 min in the presence of 0.01 M CTAB; the peaks can be easily assigned to the (100), (002), (101), (102), and (110) reflections of the hexagonal closed-packed (hcp) phase of the Co-riched NiCo alloy (JCPDS No. 89−4308), respectively. The morphology and size of the products were further examined by scanning electron microscopy (SEM), transmission electron microscopy (TEM), high-resolution transmission electron microscopy (HR-TEM), and selected-area electron diffraction (SAED). A typical SEM image shown in Figure 1b indicated that the obtained product consists of a great deal of dendrites with lengths ranging from 1 to 4 μm. A representative TEM image of an individual dendrite is shown in Figure 1c, which is in accordance with the results from SEM. Figure 1d shows a HRTEM image taken from the tip of the trunk or the branch in the panel in Figure 1c presents the lattice spacing of the typical hcp (100) fringe. The corresponding SAED pattern shown in Figure 1e was taken from the trunk tip or branch tip. The diffraction spots imply that the individual trunk or branch is single crystalline. The average length of the dendrites over the whole sample was 2.0−2.5 μm, which is in accordance with the size distribution of the dendrites (Figure 1g). The chemical composition (atomic percent) of the as-synthesized dendrites was examined by energy-dispersive X-ray (EDX) spectrometry as shown in Figure 1f. The detectable elements are nickel and cobalt, and their atomic ratio is 33.8:66.2, which is very close to the initial set ratio of Ni^{2+}/Co^{2+} = 1:2. These support that the as-prepared dendrites are pure $Ni_{33.8}Co_{66.2}$ crystals.

Temperature and Concentration of Total Metal Ion Effects. The reaction temperature and the concentration of total metal ion significantly affect the morphology of the product. Ni−Co alloy dendrites cannot be obtained at low temperature (45 °C) or high temperature (75 °C) (Figure S1 of the Supporting Information). It was found that the total concentration of metal salts were of great importance for controlling the size and morphology of the Ni−Co alloy (Figure S2 of the Supporting Information). No dendrites but nanospheres were obtained at a low metal salt concentration (Figure S2a of the Supporting Information). Well-defined dendrites were obtained when the total concentration of Ni^{2+} and Co^{2+} increased to 0.06 M (Figure S2b of the Supporting Information) and 0.12 M (Figure 1b). The dendritic structures were imperfect when the total concentration was increased to 0.18 M (Figure S2c of the Supporting Information). It was demonstrated that pure and high yield Ni−Co dendrites can be obtained only at an optimal total metal salt concentration range of 0.06−0.12 M.

Solvent and Surfactant Effects. Solvent plays very important roles for the synthesis of Ni−Co alloy structures. In order to learn more about the formation of dendrites, a number of experiments by using different solvents, such as water, methanol, *n*-propanol, *n*-butyl alcohol, and *n*-octyl alcohol, were carried out. In water, the reaction cannot occur at present conditions. Ni−Co nanoparticles with mixed hcp and fcc phases were obtained in the solvents of methanol, or *n*-butyl alcohol, or *n*-octyl alcohol (Figures S3 and S4 of the Supporting Information), while dendritic Ni−Co structure with mixed hcp and fcc phases was obtained in the solvent of *n*-propanol. These results indicated that $Ni_{33.8}Co_{66.2}$ alloy with one pure hcp phase can only be obtained in the solvent of ethanol in our experiments. The viscosity and coordinating ability of the solvents can be attribute to the effects of the reaction rate, the size, the phase, and the morphology of the alloy nanostructures, as shown in the formation of Co dendrites,[38] the solvents can control selectively the surface energy of different crystallographic faces.

The surfactant is a very important factor for preparing nano- or microstructures. Ni−Co alloy with imperfect 6-fold snowflake-like structure in mixed hcp and fcc phases in a low yield of 87 wt % was synthesized without CTAB under the same reaction conditions (Figure S5 of the Supporting Information). When the surfactant of sodium dodecyl benzenesulfonate (SDBS), sodium laurylsulfonate (SDS), polyvinylpyrrolidone (PVP), and polyethylene glycol (M_w = 20 000) (PEG-20 000) were individually employed, imperfect dendritic structures (Figure S6 of the Supporting Information) with the mixed phases of hcp and fcc Ni−Co crystals (Figure S7 of the Supporting Information) were obtained. The influence of CTAB concentration on the formation of hcp Ni−Co dendrites was also studied (Figures S8 and S9 of the Supporting Information). It has been reported that the surfactants could have several functions. The surfactants can act as a stabilizer to form a shell surrounding the particles to prevent nanoparticles from being aggregated into larger particles,[10,11,36,61−63] be thought to act as template to assemble nanomaterials with special structures,[10,11,61,64] work as capping reagents that can be selectively absorbed onto particular crystallographic facets of a growing crystal,[62] improve the yield,[36] and so forth. In the present procedure, CTAB was found to be very critical for the formation hcp phase of $Ni_{33.8}Co_{66.2}$ dendritic structures, which may play a role as a capping reagent and control the phase as well as improves the yield.

Formation Mechanism. In order to reveal the formation process of the $Ni_{33.8}Co_{66.2}$ alloy dendrites in more detail, time-dependent experiments were carried out at 55 °C in the presence of CTAB with changing reaction times from 10, 20, 30, 40, 60, 120, to 300 min while keeping all the other reaction conditions constant. The products separated from the mixtures by a magnet were hcp $Ni_{33.8}Co_{66.2}$ crystals indicated by the XRD patterns (Figure S10 of the Supporting Information) and EDX spectrometry. SEM images of the products obtained at certain reaction time intervals are shown in Figure S11 of the Supporting Information. A large number of nanoparticles and little dendrites were obtained at the early stage for 10 min (Figure S11a of the Supporting Information). The developed dendrites were obtained when the reaction time is short for 20 min (Figure S11b of the Supporting Information). If the reaction time is prolonged to 30 min, the perfect dendrites and very few snowflake dendritic structures with average diameter of 1.5−3.0 μm were obtained (Figure S11c of the Supporting Information). When the reaction time is prolonged to 40 min, we are surprised to find that the products are also composed dendrites and more snowflakelike dendritic structures (Figure S11d of the Supporting Information). If the reaction time is extended to 60 min, a big number of snowflake and few single dendritic structures were obtained (Figure S11e of the Supporting Information). When the reaction time is further prolonged to 120 min, the products were composed of snowflakelike and very few single dendritic structures (Figure S11f of the Supporting Information). But when the reaction time is prolonged to 300 min, the snowflakes were imperfect (Figure S11g of the Supporting Information). These results indicate a proper reaction time is very important for forming perfect dendritic structures.

Several models including diffusion limited aggregation (DLA),[65,66] and cluster−cluster aggregation (CCA)[66,67] have been widely used to explain and analyze the formation of dendritic crystals in nonequilibrium systems. Generally, single crystalline

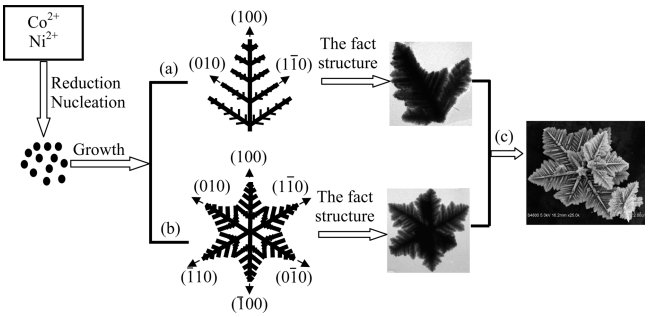

Figure 2. Schematic illustration of the formation process of the dendrites and snowflakelike structures: (a) fast growth along one direction; (b) fast growth along six equivalent directions; (c) Ostwald ripening formation of snowflakelike structures.

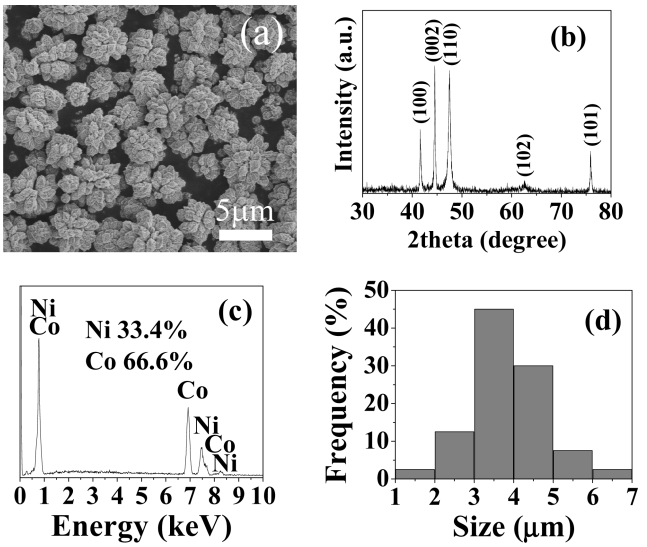

Figure 3. Integrated characterization of flowerlike $Ni_{33.4}Co_{66.6}$ obtained by a SDBS assisted hydrothermal route: (a) SEM image; (b) XRD pattern; (c) EDX spectrum; (d) size distribution.

dendritic fractals have crystallographically equivalent growth direction, usually [100] for cubic phase and [1$\bar{1}$00] for hexagonal phase.[37] Ethanol solution provides a good environment for the diffusion of nuclei, which is favorable for the dendrites.[38] From the time-dependent experiments, the possible growth mechanism of $Ni_{33.8}Co_{66.2}$ alloy dendrites and snowflakelike structures could be explained by the model proposed in Figure 2, which is similar to the reported α-Fe_2O_3 dendritic micropine.[68] It is proposed that CTAB controlled kinetically the growth rates of different crystalline faces ($\bar{1}$00), ($\bar{1}$10), and (0$\bar{1}$0) of the $Ni_{33.8}Co_{66.2}$ alloy by interacting with these faces through adsorption and desorption and then the dendrites were obtained.

Flowerlike Ni−Co Alloys. Flowerlike $Ni_{33.4}Co_{66.6}$ with hcp phase in size of 2.5−5.5 μm were synthesized in the solvent of ethanol in the presence of sodium dodecyl benzenesulfonate (SDBS) by a solvothermal process at 120 °C for 10 h (Figure 3). Surfactant SDBS and solvent ethanol played critical roles for the flowerlike NiCo structures.[69]

Magnetic Property. The magnetic properties of the as-synthesized $NiCo_2$ structures, namely, $Ni_{33.8}Co_{66.2}$ dendrites in length of 1.5−3.0 μm and flowerlike $Ni_{33.4}Co_{66.6}$ in diameter

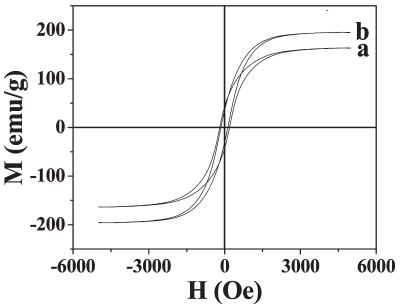

Figure 4. Room temperature magnetic hysteresis loops of (a) $Ni_{33.8}Co_{66.2}$ dendrites and (b) flowerlike $Ni_{33.4}Co_{66.6}$.

of 2.5−5.5 μm, were investigated at room temperature using a vibrating sample magnetometer (VSM, BHV-55) with an applied field of −5 kOe < H < 5 kOe. The samples were first quantified carefully and then sealed into plastic tubes for the magnetization measurements. The hysteresis loop of the samples shown in Figure 4 revealed that both of the $NiCo_2$ structures are ferromagnetic at room temperature. The saturation magnetization (Ms), remanent magnetization (Mr), and coercivity (Hc) values for the each $NiCo_2$ structure are shown in Table S1 of the Supporting Information. The saturation magnetization value of the $Ni_{33.8}Co_{66.2}$ dendrites (163.55 emu/g) is lower than that of the flowerlike $Ni_{33.4}Co_{66.6}$ (195.79 emu/g). Surface oxidation at grain boundaries and the large surface to-volume ratio may be the reason to cause a decrease in saturation magnetization.[70] On the other hand, compared to the coercivity value of flowerlike $Ni_{33.4}Co_{66.6}$ (147.77 Oe), the $Ni_{33.8}Co_{66.2}$ dendritic structures exhibited an enhanced value (192.35 Oe). The larger coercivity of the $Ni_{33.8}Co_{66.2}$ dendrites is considered to be attributed to the intrinsic large magnetocrystalline anisotropy of ordered intermetallic compound and also mainly due to the effect of size, shape, and structure.[44] Certainly, these are not the only parameters that we have to consider. The composition, internal stress, and defects also influence this value. Our experimental results give a hint that the magnetic properties of $Ni_{33.8}Co_{66.2}$ dendrites may be explained considering crystalline anisotropy and shape anisotropy, as similar to the $FeNi_3$ and cobalt dendrites,[35,38,39] which need to be investigated further.

Catalytic Activity to the 4-NP Reduction. Reduction of aromatic nitro compounds to their corresponding amino derivatives is industrially important whereas the aromatic nitro compounds are normally not reduced by sodium borohydride in aqueous or alcoholic solution. Under a neutral or acidic condition, 4-NP solution exhibits a strong absorption peak at 317 nm.[47] Upon the addition of $NaBH_4$, the alkalinity of the solution increased, and 4-NP ions would become the dominating species, together with a spectral shift to 400 nm for the absorption peak.[40,45,47] After the $NiCo_2$ alloys catalyst was added (i.e., an aqueous dispersion of the $Ni_{33.8}Co_{66.2}$ dendrites or flowerlike $Ni_{33.4}Co_{66.6}$), the absorption peak at 400 nm gradually dropped in intensity as the reduction reaction proceeded (Figure 5). At the same time, with the production of 4-AP, a new absorption peak started to rise as a shoulder at 315 nm.[40,45,47] Since the peak at 400 nm was much stronger than that at 315 nm, the concentrations of 4-NP ions were measured, and the progress or kinetics of the reaction were monitored by recording the absorbance at 400 nm. For all experiments, the initial concentrations of 4-NP, $NiCo_2$ catalysts, and $NaBH_4$

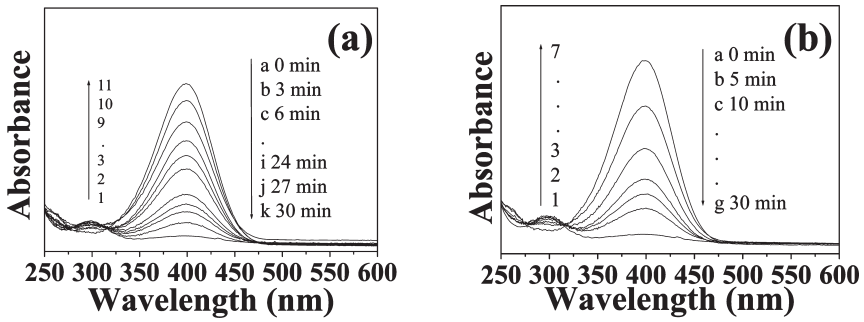

Figure 5. Typical UV−vis spectra for the successive reduction of 4-NP by $NaBH_4$ using $Ni_{33.8}Co_{66.2}$ dendrites and flowerlike $Ni_{33.4}Co_{66.6}$ as catalysts with IT of 100 and 120 s, respectively. Condition: [4-NP], 1.0×10^{-4} M; [$NaBH_4$], 6.0×10^{-2} M; catalyst, 100 mg/L; 20 °C.

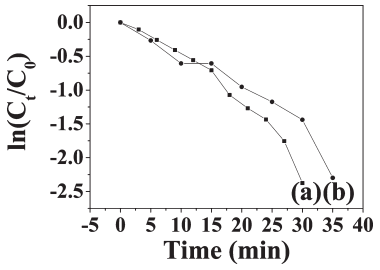

Figure 6. Plots of $\ln(C_t/C_0)$ versus time for each $NiCo_2$ alloy with different morphologies at 20 °C: (a) $Ni_{33.8}Co_{66.2}$ dendrites; (b) flowerlike $Ni_{33.4}Co_{66.6}$. Condition: [4-NP], 1.0×10^{-4} M; [$NaBH_4$], 6×10^{-2} M; [catalyst], 100 mg/L.

were kept at 1.0×10^{-4} M, 100 mg/L, and 6.0×10^{-2} M, respectively.

Figure 5 shows a typical UV−vis absorption change of the reaction mixture by the addition of $NiCo_2$ alloys as the solid phase catalyst at the temperature of 20 °C. Without the addition of $NiCo_2$ alloy catalyst, no reaction was observed even for a couple of days. This observation indicates that the reduction reaction was unable to occur by itself under the experimental conditions. Upon the addition of a $NiCo_2$ alloy catalyst, regardless of the morphology, a certain period of time was required for the 4-NP to adsorb onto the catalyst's surface before the reaction could be initiated, which is called the induction time (IT).[47,49] Among the different systems, the reaction catalyzed by $Ni_{33.8}Co_{66.2}$ dendrites showed the shorter IT (100 s) as compared to flowerlike $Ni_{33.4}Co_{66.6}$ (120 s). We assumed that the rate of adsorption of 4-NP on the surface of a catalyst is the predominant factor in the induction period. The adsorption of 4-NP might play an important role in activating the reaction. Accordingly, it is not difficult to understand why the larger specific surface area the catalyst possesses, the faster the reactant will be activated, and the shorter the induction period will be.

The UV−vis spectra also exhibit an isosbestic point between two absorption bands (Figure 5), indicating that only two principal species, 4-NP and 4-AP, influence the reaction kinetics.[53,55] Therefore, the rate constants of reducing 4-NP to 4-AP could be evaluated by pseudofirst-order kinetics when excess $NaBH_4$ was used.[47−50,53,55] In our reaction system, with the different shapes of NiCo alloys, the ratio of C_t and C_0, where C_t and C_0 are 4-NP concentrations at time t and 0, respectively, was measured from the relative intensity of the respective absorbances at 400 nm, A_t/A_0.[53] The approximately linear relations of $\ln(C_t/C_0)$ versus time were observed for both catalysts as shown in Figure 6, supporting pseudofirst-order kinetics. We calculated the average reaction rate constants (k) at 20 °C are 0.07348 min^{-1} for the $Ni_{33.8}Co_{66.2}$ dendrites and 0.05717 min^{-1} for the flowerlike $Ni_{33.4}Co_{66.6}$, which indicated a higher catalytic activity for the $Ni_{33.8}Co_{66.2}$ dendrites as they have more surface-to-volume ratio and surface areas under the nearly same sizes, since the Brunauer−Emmett−Teller (BET) surface areas were determined as 32.68 m^2/g for the $Ni_{33.8}Co_{66.2}$ dendrites and 20.66 m^2/g for the flowerlike $Ni_{33.4}Co_{66.6}$.

It is noted that no trace of Ni(II) and Co(II) was observed after the reduction of nitro compound, which is similar to the situation of Pt−Ni bimetallic nanoparticles but different to that of Raney Ni.[55] Through the experimental results, we know that the $NiCo_2$ alloys are good catalysts with characters of low cost, reused, fast, and magnetic separation for the reduction of 4-NP into 4-AP by $NaBH_4$, and the rate constants exhibited a shape-dependent catalytic property that is similar to Au-based nanocages, nanoboxes, and nanoparticles.[47]

CONCLUSIONS

In conclusion, we report a solution phase chemical route to synthesize dendritic and flowerlike hcp phase $NiCo_2$ alloy microstructures, which is a simple, fast, low cost, and practical method for large-scale preparation. The morphology and crystal phase of Ni−Co can be controlled by adjusting the reaction temperature, the total concentration of [Ni^{2+}] + [Co^{2+}], the kinds of solvent and surfactants, and so forth. Magnetic measurements revealed that $Ni_{33.8}Co_{66.2}$ dendrites have a lower saturation magnetization value than that of the flowerlike $Ni_{33.4}Co_{66.6}$ but exhibit an enhanced coercivity value. We have demonstrated the use of $NiCo_2$ alloys with different shapes as new reusable heterogeneous catalysts for the reduction of 4-nitrophenol by $NaBH_4$, and the rate constants exhibited shape-dependent catalytic properties: $Ni_{33.8}Co_{66.2}$ dendrites are catalytically more active than the flowerlike $Ni_{33.4}Co_{66.6}$. Given the ferromagnetism and abundance as well as the easiness in controlling the morphology and structures, the Ni−Co based microstructures might be able to find widespread use as catalysts in a number of industry applications.

ASSOCIATED CONTENT

Supporting Information. Magnetic data of $Ni_{33.8}Co_{66.2}$ dendrites and flowerlike $Ni_{33.4}Co_{66.6}$ at room temperature, and additional characterizations by SEM and XRD. This material is available free of charge via the Internet at http://pubs.acs.org.

AUTHOR INFORMATION

Corresponding Author

*Fax: 86 5533869303; Phone: 86 5533937137; E-mail: xwwei@mail.ahnu.edu.cn.

ACKNOWLEDGMENT

This work is supported by Science and Technological Fund of Anhui Province for Outstanding Youth (No. 08040106906), the National Natural Science Foundation (Nos. 21071005, 2049-0217, and 20671002) of P. R. China, the State Education Ministry (EYTP, SRF for ROCS, SRFDP 20070370001), and the Education Department (Nos. 2006KJ006TD, 2008Z028) of Anhui Province.

REFERENCES

(1) Singh, V. B.; Singh, V. N. *Plat. Surf. Finish.* **1976**, *63*, 34–36.

(2) Masoeroa, A.; Morten, B.; Olcesec, G. L.; Prudenziatib, M.; Tango, F.; Vinai, F. *Thin Solid Films* **1999**, *350*, 214–218.

(3) Kritzer, P.; Boukis, N.; Dinjus, E. *Corrosion* **2000**, *56*, 1093–1104.

(4) Mercier, D.; Lévy, J.-C. S.; Viau, G.; Fiévet-Vincent, F.; Fiévet, F. *Phys. Rev. B* **2000**, *62*, 532–544.

(5) Wang, L.; Gao, Y.; Xue, Q.; Liu, H.; Xu, T. *Appl. Surf. Sci.* **2005**, *242*, 326–332.

(6) Domínguez-Crespo, M. A.; Plata-Torres, M.; Torres-Huerta, A. M.; Arce-Estrada, E. M.; Hallen-López, J. M. *Mater. Charact.* **2005**, *55*, 83–91.

(7) (a) Chi, B.; Li, J.; Yang, X.; Gong, Y.; Wang, N. *Int. J. Hydrogen Energy* **2005**, *30*, 29–34. (b) Hibbard, G. D.; Aust, K. T.; Erb, U. *Mater. Sci. Eng., A* **2006**, *433*, 195–202. (c) Gu, C.; Lian, J.; Jiang, Z. *Adv. Eng. Mater.* **2006**, *8*, 252–256.

(8) Atkinson, A.; Barnett, S.; Gorte, R. J.; Irvine, J. T. S.; McEvoy, A. J.; Mogensen, M.; Singhal, S. C.; Vohs, J. *Nat. Mater.* **2004**, *3*, 17–27.

(9) (a) Zhang, L.; Bain, J. A.; Zhu, J. -G.; Abelmann, L.; Onoue, T. *J. Appl. Phys.* **2006**, *100*, 053901–053905. (b) Onoue, T.; Siekman, M. H.; Abelmann, L. *J. Magn. Magn. Mater.* **2005**, *287*, 501–506.

(10) Hu, M. J.; Lu, Y.; Zhang, S.; Guo, S. R.; Lin, B.; Zheng, M.; Yu, S. H. *J. Am. Chem. Soc.* **2008**, *130*, 11606–11607.

(11) (a) Hu, M. J.; Lin, B.; Yu, S. H. *Nano Res.* **2008**, *1*, 303–313. (b) Zhu, L. P.; Xiao, H. M.; Fu, S. Y. *Eur. J. Inorg. Chem.* **2007**, 3947–3951.

(12) Ung, D.; Soumare, Y.; Chakroune, N.; Viau, G.; Vaulay, M. J.; Richard, V.; Fiévet, F. *Chem. Mater.* **2007**, *19*, 2084–2094.

(13) Elumalai, P.; Vasan, H. N.; Verelst, M.; Lecante, P.; Carles, V.; Taihades, P. *Mater. Res. Bull.* **2002**, *37*, 353–363.

(14) Qin, D. H.; Wang, C. W.; Sun, Q. Y.; Li, H. L. *Appl. Phys. A: Mater. Sci. Process.* **2002**, *74*, 761–765.

(15) Ung, D.; Viau, G.; Ricolleau, C.; Warmont, F.; Gredin, P.; Fiévet, F. *Adv. Mater.* **2005**, *17*, 338–344.

(16) Thongmee, S.; Pang, H. L.; Yi, J. B.; Ding, J.; Lin, J. Y.; Van, L. H. *Acta Mater.* **2009**, *57*, 2482–2487.

(17) Li, X. Z.; Wei, X. W.; Ye, Y. *Mater. Lett.* **2009**, *63*, 578–580.

(18) Zhang, D. E.; Ni, X. M.; Zhang, X. J.; Zheng, H. G. *J. Magn. Magn. Mater.* **2006**, *302*, 290–293.

(19) Wen, M.; Wang, Y. F.; Zhang, F.; Wu, Q. S. *J. Phys. Chem. C* **2009**, *113*, 5960–5966.

(20) Jang, H. C.; Ju, S. H.; Kang, Y. C. *J. Alloys Compd.* **2009**, *478*, 206–209.

(21) Li, Y. D.; Li, L. Q.; Liao, H. W.; Wang, H. R. *J. Mater. Chem.* **1999**, *9*, 2675–2677.

(22) Sangregorio, C.; Julián Fernández, C.; Battaglin, G.; De, G.; Gatteeschi, D.; Mattei, G.; Mazzoldi, P. *J. Magn. Magn. Mater.* **2004**, *272*, e1251–e1252.

(23) (a) Brayner, R.; Vaulay, M. J.; Fiévet, F.; Coradin, T. *Chem. Mater.* **2007**, *19*, 1190–1198. (b) Ahmed, J.; Sharma, S.; Ramanujachary, K. V.; Lofland, S. E.; Ganguli, A. K. *J. Colloid Interface Sci.* **2009**, *336*, 814–819. (c) Toneguzzo, P.; Viau, G.; Acher, O.; Guillet, F.; Bruneton, E.; Fievet-Vincent, F.; Fievet, F. *J. Mater. Sci.* **2000**, *35*, 3767–3784.

(24) Naoufal, B.; Peter, A. P.; Zhen, T.; Xin, H.; Fei, Q.; Kantharina, K.-H. *Chem. Mater.* **2010**, *22*, 92–100.

(25) (a) Elbuken, C.; Yavuz, M.; Khamesee, M. B. *J. Appl. Phys.* **2008**, *104*, 044905–044911. (b) Qiao, G.; Jing, T.; Wang, N.; Gao, Y.; Zhao, X.; Zhou, J.; Wang, W. *Electrochim. Acta* **2005**, *51*, 85–92.

(26) (a) Tomita, S.; Adachi, H.; Fujii, M.; Hayashi, S. *J. Appl. Phys., Part 1* **2001**, *40*, 6370–6374. (b) Chung, C. K.; Chang, W. T. *Thin Solid Films* **2009**, *517*, 4800–4804.

(27) (a) Kodama, D.; Shinoda, K.; Sato, K.; Konno, Y.; Joseyphus, R. J.; Motomiya, K.; Takahashi, H.; Matsumoto, T.; Sato, Y.; Tohji, K.; Jeyadevan, B. *Adv. Mater.* **2006**, *18*, 3154–3159. (b) Su, X.; Zheng, H.; Yang, Z.; Zhu, Y.; Pan, A. *J. Mater. Sci.* **2003**, *38*, 4581–4585.

(28) Wang, J.; Asmussen, R. M.; Adams, B.; Thomas, D. F.; Chen, A. *Chem. Mater.* **2009**, *21*, 1716–1724.

(29) Qiu, R.; Zhang, X. L.; Qiao, R.; Li, Y.; Kim, Y. I.; Kang, Y. S. *Chem. Mater.* **2007**, *19*, 4174–4180.

(30) Adams, B. D.; Wu, G. S.; Nigro, S.; Chen, A. *J. Am. Chem. Soc.* **2009**, *131*, 6930–6931.

(31) Zhou, P.; Dai, Z. H.; Fang, M.; Huang, X. H.; Bao, J. C.; Gong, J. F. *J. Phys. Chem. C* **2007**, *111*, 12609–12616.

(32) (a) Song, Y.; Kim, J. Y.; Park, K. W. *Cryst. Growth Des.* **2009**, *9*, 505–507. (b) Xiao, J. P.; Xie, Y.; Tang, R.; Chen, M.; Tian, X. B. *Adv. Mater.* **2001**, *13*, 1887–1891.

(33) (a) Brennan, M. E.; Whelan, A. M.; Kelly, J. M.; Blau, W. J. *Synth. Met.* **2005**, *154*, 205–208. (b) Wei, G. D.; Nan, C. W.; Deng, Y.; Lin, Y. H. *Chem. Mater.* **2003**, *15*, 4436–4441. (c) Lu, L. H.; Kobayashi, A.; Kikkawa, Y.; Tawa, K.; Ozaki, Y. *J. Phys. Chem. B* **2006**, *110*, 23234–23241. (d) Han, Y.; Liu, S.; Han, M.; Bao, J.; Dai, Z. *Cryst. Growth Des.* **2009**, *9*, 3941–3947. (e) Wen, X.; Xie, Y. T.; Mak, M. W. C.; Cheung, K. Y.; Li, X. Y.; Renneberg, R.; Yang, S. *Langmuir* **2006**, *22*, 4836–4842. (f) Cho, E. J.; Kang, J. K.; Han, W. S.; Jung, J. H. *Langmuir* **2008**, *24*, 5229–5232.

(34) (a) Sun, X. P.; Hagner, M. *Langmuir* **2007**, *23*, 9147–9150. (b) Huang, T.; Meng, F.; Qi, L. *Langmuir* **2010**, *26*, 7582–7589.

(35) Qin, Y.; Song, Y.; Sun, N.; Zhao, N.; Li, M.; Qi, L. *Chem. Mater.* **2008**, *20*, 3965–3972.

(36) Liu, X. M.; Fu, S. Y. *J. Cryst. Growth* **2007**, *306*, 428–432.

(37) Ye, J.; Chen, Q. W.; Qi, H. P.; Tao, N. *Cryst. Growth Des.* **2008**, *8*, 2464–2468.

(38) Zhu, Y. C.; Zheng, H. G.; Yang, Q.; Pan, A. L.; Yang, Z. P.; Qian, Y. T. *J. Cryst. Growth* **2004**, *260*, 427–434.

(39) (a) Zhu, G. X.; Wei, X. W.; Xia, C. J.; Ye, Y. *Carbon* **2007**, *45*, 1160–1166. (b) Liu, X. H.; Yi, R.; Wang, Y. T.; Qiu, G. Z.; Zhang, N.; Li, X. G. *J. Phys. Chem. C* **2007**, *111*, 163–167. (c) Zhu, L. P.; Xiao, H. M.; Zhang, W. D.; Yang, Y.; Fu, S. Y. *Cryst. Growth Des.* **2008**, *8*, 1113–1118.

(40) Yan, C. L.; Xue, D. F. *Cryst. Growth Des.* **2008**, *8*, 1849–1854.

(41) (a) Zhang, X.; Wang, G.; Liu, X.; Wu, H.; Fang, B. *Cryst. Growth Des.* **2008**, *8*, 1430–1434. (b) Qiu, R.; Cha, H. G.; Noh, H. B.; Shim, Y. B.; Zhang, X. L.; Qiao, R.; Zhang, D.; Kim, Y.; Pal, U.; Kang, Y. S. *J. Phys. Chem. C* **2009**, *113*, 15891–15896. (c) Panda, B. R.; Rao, P. N.; Paul, A.; Chattopadhyay, A. *J. Phys. Chem. B* **2006**, *110*, 22917–22922.

(42) Li, G. R.; Yao, C. Z.; Lu, X. H.; Zheng, F. L.; Feng, Z. P.; Yu, X. L.; Su, C. Y.; Tong, Y. X. *Chem. Mater.* **2008**, *20*, 3306–3314.

(43) Wang, D. W.; Li, T.; Liu, Y.; Huang, J. S.; You, T. Y. *Cryst. Growth Des.* **2009**, *9*, 4351–4355.

(44) Zhou, X. M.; Wei, X. W. *Cryst. Growth Des.* **2009**, *9*, 7–12.

(45) Praharaj, S.; Nath, S.; Ghosh, S. K.; Kundu, S.; Pal, T. *Langmuir* **2004**, *20*, 9889–9892.

(46) (a) Sau, T. K.; Pal, A.; Pal, T. *J. Phys. Chem. B* **2001**, *105*, 9266–9272. (b) Esumi, K.; Miyamoto, K.; Yoshimura, T. *J. Colloid Interface Sci.* **2002**, *254*, 402–405. (c) Hayakawa, K.; Yoshimura, T.; Esumi, K. *Langmuir* **2003**, *19*, 5517–5521. (d) Panigrahi, S.; Basu, S.; Praharaj, S.; Pande, S.; Jana, S.; Pal, A.; Ghosh, S. K.; Pal, T. *J. Phys. Chem.*

C **2007**, *111*, 4596–4605. (e) Corma, A.; Concepción, P.; Serna, P. *Angew. Chem., Int. Ed.* **2007**, *46*, 7266–7269.
(47) Zeng, J.; Zhang, Q.; Chen, J. Y.; Xia, Y. N. *Nano Lett.* **2010**, *10*, 30–35.
(48) Saha, S.; Pal, A.; Kundu, S.; Basu, S.; Pal, T. *Langmuir* **2010**, *26*, 2885–2893.
(49) Pradhan, N.; Pal, A.; Pal, T. *Collioids Surf., A* **2002**, *196*, 247–257.
(50) Jana, S.; Ghosh, S. K.; Nath, S.; Pande, S.; Praharaj, S.; Panigrahi, S.; Basu, S.; Endo, T.; Pal, T. *Appl. Catal., A* **2006**, *313*, 41–48.
(51) Xu, S. G.; Xi, X. L.; Cao, S. K. *J. Mol. Catal. A: Chem.* **2000**, *160*, 287–292.
(52) Min, K. I.; Choi, J. S.; Chung, Y. M.; Ahn, W. S.; Ryoo, R.; Lim, P. K. *Appl. Catal., A* **2008**, *337*, 97–104.
(53) Lee, J.; Park, J. C.; Song, H. *Adv. Mater.* **2008**, *20*, 1523–1528.
(54) Zhang, H.; Li, X.; Chen, G. *J. Mater. Chem.* **2009**, *19*, 8223–8231.
(55) Ghosh, S. K.; Mandal, M.; Kundu, S.; Nath, S.; Pal, T. *Appl. Catal., A* **2004**, *268*, 61–66.
(56) Sugimori, A. *Bull. Chem. Soc. Jpn.* **1961**, *34*, 407–411.
(57) Chen, R.; Wang, Q.; Du, Y.; Xing, W.; Xu, N. *Chem. Eng. J.* **2009**, *145*, 371–376.
(58) Chen, R.; Du, Y.; Xing, W.; Xu, N. *Chin. J. Chem. Eng.* **2007**, *15*, 884–888.
(59) Chen, R.; Du, Y.; Xing, W.; Xu, N. *Chin. J. Chem. Eng.* **2006**, *14*, 665–669.
(60) Goswami, N.; Rahman, M. L.; Huque, M. E.; Qaisuddin, M. *Chem. Technol. Biotechnol.* **1984**, *34*, 195–202.
(61) Guo, L.; Liang, F.; Wen, X.; Yang, S.; He, L.; Zheng, W.; Chen, C.; Zhong, Q. *Adv. Funct. Mater.* **2007**, *17*, 425–430.
(62) (a) Zhu, L. P.; Zhang, W. D.; Xiao, H. M.; Yang, Y.; Fu, S. Y. *J. Phys. Chem. C* **2008**, *112*, 10073–10078. (b) Liu, Z. P.; Li, S.; Yang, Y.; Peng, S.; Hu, Z. K.; Qian, Y. T. *Adv. Mater.* **2003**, *15*, 1946–1948.
(63) (a) Han, M. Y.; Quek, C. H. *Langmuir* **2000**, *16*, 362–367. (b) Chen, W. X.; Lee, J. Y.; Liu, Z. L. *Chem. Commun.* **2002**, 2588–2589. (c) Narayanan, R.; El-Sayed, M. A. *J. Am. Chem. Soc.* **2003**, *125*, 8340–8347. (d) Yin, B. S.; Ma, H. Y.; Wang, S. Y.; Chen, S. H. *J. Phys. Chem. B* **2003**, *107*, 8898–8904. (e) Zhang, D.; Ni, X.; Zheng, H. *J. Colloid Interface Sci.* **2005**, *292*, 410–412. (e) Jia, Z. J.; Zhu, L. P.; Liao, G. H.; Yu, Y.; Tang, Y. W. *Solid State Commun.* **2004**, *132*, 78–82.
(64) (a) Xie, Q.; Dai, Z.; Huang, W. W.; Liang, J. B.; Jiang, C. L.; Qian, Y. T. *Nanotechnology* **2005**, *16*, 2958–2962. (b) Yu, Y.; Du, F. P.; Yu, J. C.; Zhuang, Y. Y.; Wong, P. *J. Solid State Chem.* **2004**, *177*, 4640–4647. (c) Peng, X. G.; Manna, L.; Yang, W. D.; Wickham, J.; Scher, E.; Kadavanich, A.; Alivisatos, A. P. *Nature* **2000**, *404*, 59–61. (d) Tang, Z. Y.; Kotov, N. A.; Giersig, M. *Science* **2002**, *297*, 237–240.
(65) (a) Witten, T. A.; Sander, L. M. *Phys. Rev. Lett.* **1981**, *47*, 1400–1403. (b) Halsey, T. C.; Duplantier, B.; Honda, K. *Phys. Rev. Lett.* **1997**, *78*, 1719–1722.
(66) Fang, X. J.; You, H. J.; Kong, P.; Yi, Y.; Song, X. P.; Ding, B. J. *Cryst. Growth Des.* **2007**, *7*, 864–867.
(67) (a) Meakin, P. *Phys. Rev. Lett.* **1983**, *51*, 1119–1122. (b) Kolb, M.; Botet, R.; Jullien, R. *Phys. Rev. Lett.* **1983**, *51*, 1123–1126.
(68) Cao, M. H.; Liu, T. F.; Gao, S.; Sun, G. B.; Wu, X. L.; Hu, C. W.; Wang, Z. L. *Angew. Chem., Int. Ed.* **2005**, *44*, 2–6.
(69) Wei, X. W.; Zhou, X. M.; Wu, K. L.; Chen, Y. *CrystEngComm* **2011**, *13*, 1328–1332.
(70) (a) Wei, X. W.; Zhu, G. X.; Zhou, J. H.; Sun, H. Q. *Mater. Chem. Phys.* **2006**, *100*, 481–485. (b) Hausmanns, B.; Krome, T. P.; Dumpich, G. *J. Appl. Phys.* **2003**, *93*, 8095–8097.